TRANSIENT SPATIOTEMPORAL CHAOS IS EXTENSIVE IN THREE REACTION-DIFFUSION NETWORKS

By

Daniel Stahlke

RECOMMENDED:

_____

_____

_____

Advisory Committee Chair

_____

Chair, Department of Physics

APPROVED:

_____

Dean, College of Natural Science and Mathematics

_____

Dean of the Graduate School

_____

Date

TRANSIENT SPATIOTEMPORAL CHAOS IS EXTENSIVE IN THREE REACTION-DIFFUSION NETWORKS

A

THESIS

Presented to the Faculty

of the University of Alaska Fairbanks

in Partial Fulfillment of the Requirements

for the Degree of

MASTER OF SCIENCE

By

Daniel Stahlke, B.S.

Fairbanks, Alaska

May 2010

Abstract

Extensive (asymptotic) spatiotemporal chaos is comprised of statistically similar subsystems that interact only weakly. A systematic study of transient spatiotemporal chaos reveals extensive system behavior in all three reaction-diffusion networks for various boundary conditions. The Lyapunov dimension, the sum of positive Lyapunov exponents, and the logarithm of the transient lifetime grow linearly with system size. The unstable manifold of the chaotic saddle has nearly the same dimension as the saddle itself, and the stable manifold is nearly space filling. The majority of this work is published in D. Stahlke and R. Wackerbauer. *Phys. Rev. E*, 80(5):056211, 2009.[1].

Table of Contents **Page**

List of Figures **Page**

List of Tables **Page**

Acknowledgements

This research is based upon work supported by the National Science Foundation under grant number PHY-0653086, and by the Arctic Region Supercomputing Center at the University of Alaska Fairbanks as part of the Department of Defense High Performance Computing Modernization Program.

Chapter 1
Introduction

Transient spatiotemporal chaos is a generic pattern in extended non-equilibrium systems in which spatiotemporal dynamics spontaneously changes from chaotic to regular (steady state or periodic) behavior. Transient spatiotemporal chaos was found in models for semi-conductor charge transport [2], for the CO oxidation on single-crystal Pt surfaces [3], for a cubic autocatalytic reaction [4], in models of turbulent dynamics [5, 6], and in systems of coupled logistic maps [7, 8]. Experimental studies show that turbulence in shear flow is transient [9]. "Stable chaos" (with a negative Lyapunov exponent) is transient in systems of coupled one-dimensional maps [10].

Extended chaotic systems that have no long-range interactions are expected to be uncorrelated at large length scales and therefore should behave as a sum of their parts [11]. Then spatiotemporal chaos is extensive, and the spectrum of Lyapunov exponents converges to a function that is intensive. This implies that the attractor dimension (Lyapunov dimension) grows in direct proportion to the volume of the system [12, 13]. While extensivity in (asymptotic) spatiotemporal chaos has been studied for a while [12, 13, 14, 15, 16, 17], extensivity in transient spatiotemporal chaos is rather unexplored [3, 18].

The average lifetime of transient spatiotemporal chaos typically grows exponentially with the volume of the system [4, 19, 20]. The origin of this exponential scaling is most likely due to the probability for randomly uncorrelated regions generating a global pattern that initiates the collapse of spatiotemporal chaos [21, 2, 18]. This feature of transient spatiotemporal chaos particularly motivates more detailed studies on extensive properties in transient dynamics.

This paper systematically explores and verifies extensivity of transient spatiotemporal chaos in three reaction-diffusion networks and a variety of boundary conditions. Section II introduces the three excitable reaction-diffusion networks with Gray-Scott reaction dynamics [22], with Bär-Eiswirth reaction dynamics [23], and with Wacker-Schöll reaction dynamics [2]. The lifetime of transient spatiotemporal chaos is discussed in Sect III, and the Lyapunov spectra and dimensions are investigated in Sect. IV. Section V describes dimensional properties of the chaotic saddle, and Sect. VI focuses on various densities and their qualitative statistical interpretations.

Chapter 2

Reaction-diffusion networks

The networks consist of N diffusively coupled, identical, continuous-time dynamical elements. At each network node $n\,(n = 1, 2, \ldots N)$ the uncoupled dynamics is given by $\frac{d\mathbf{x}_n}{dt} = \mathbf{F}(\mathbf{x}_n)$ with $\mathbf{x}_n$ a d-dimensional state vector. The reaction-diffusion network is given by

$$\frac{d\mathbf{x}_n}{dt} = \mathbf{F}(\mathbf{x}_n) + D\sum_{j=1}^{N} G_{nj} H \mathbf{x}_j. \tag{2.1}$$

D is a global coupling parameter. H is a $d \times d$ diagonal matrix representing the relative diffusion of each species. G is an $N \times N$ symmetric Laplacian matrix required to meet the condition $\sum_{j=1}^{N} G_{ij} = 0$. For a regular network in one dimension the coupling matrix G is

$$G_{ij} = \nabla^2_{ij} = \delta_{i,j-1} - 2\delta_{ij} + \delta_{i,j+1}, \tag{2.2}$$

with $i, j = 1, 2, \ldots N$. The indices are equivalent modulo N for periodic boundary conditions and $G_{i1} = \delta_{i2} - \delta_{i1}$ and $G_{iN} = \delta_{i,N-1} - \delta_{iN}$ for no-flux boundary conditions. In the presence of a single shortcut of length k between node 1 and $k + 1$ the coupling matrix becomes

$$G_{ij} = \nabla^2_{ij} + \delta_{i1}(\delta_{j,k+1} - \delta_{ij}) + \delta_{i,k+1}(\delta_{j1} - \delta_{ij}). \tag{2.3}$$

The coupling strength parameter D controls the characteristic length scale. From the rescaling of Eq. (2.1) it follows that the general characteristics of the system remain the same if N and D are both increased while holding $N/\sqrt{D}$ constant. If N goes to infinity with $N/\sqrt{D}$ held constant the system approaches a continuous form. On the other hand if N (and hence D) is made too small discretization effects will start to become significant and eventually the system will no longer be able to support chaos. In this paper D is large enough for the networks to be good approximations for the continuum system, except where noted otherwise.

We consider three excitable dynamical systems F: the Gray-Scott (GS) system [22], the Bär-Eiswirth (BE) system [23], and the Wacker-Schöll (WS) system [2]. Each of the systems consist of two species ($d = 2$), so each $\mathbf{x}_n$ is a two-dimensional vector. Thus the uncoupled system does not exhibit chaos, and spatiotemporal chaos is induced by the diffusive coupling of the excitable dynamical elements in Eq. (2.1).

The *Gray-Scott system* [22] represents an open autocatalytic reaction $A + 2B \rightarrow 3B$ and $B \rightarrow C$. The equations are

$$\mathbf{F}\left(\begin{bmatrix} a \\ b \end{bmatrix}\right) = \begin{bmatrix} 1 - a - \mu ab^2 \\ \mu ab^2 - \Phi b \end{bmatrix} \text{ and } H = \begin{bmatrix} 1 & 0 \\ 0 & 1 \end{bmatrix}, \tag{2.4}$$

where a and b are dimensionless species concentrations, and ϕ and μ are bifurcation parameters. In the parameter regime of coupling-induced spatiotemporal chaos the function $\mathbf{F}$ has three fixed points: $S^n = (1, 0)$ is a stable node that exists for all values of ϕ and μ, and the additional fixed points $S^f = \left(\frac{1-\sqrt{1-4\phi^2/\mu}}{2}, \frac{1+\sqrt{1-4\phi^2/\mu}}{2\phi}\right)$ and $S^s = \left(\frac{1+\sqrt{1-4\phi^2/\mu}}{2}, \frac{1-\sqrt{1-4\phi^2/\mu}}{2\phi}\right)$ exist for values of μ above the saddle node bifurcation point $\mu_{sn} = 4\phi^2$. When $\mu > \mu_{sn}$, S^s is a saddle point and within the range $2 < \phi < 4$, S^f is an unstable focus for values of μ below the subcritical Hopf bifurcation point $\mu_H = \phi^4/(\phi - 1)$. The parameter range $[\mu_c, \mu_H]$ yields wave induced spatiotemporal chaos, with μ_c being the critical threshold for traveling wave solutions [4]. For $\phi = 2.8$, $\mu_c \approx 33$ and $\mu_H \approx 34.1$. In the Gray-Scott network [Eqs. (2.1, 2.4)] the spatiotemporal chaos is Šilnikov-like; a typical trajectory at a network node spirals away from the unstable focus toward the stable node, and then is reinjected into the neighborhood of the unstable focus by the propagating reaction-diffusion front [24]. For the calculations in this paper we have used the parameters $\mu \in \{33.5, 33.7, 33.9\}$ and $\Phi = 2.8$.

The *Bär-Eiswirth system* [23] describes a surface reaction model for the oxidation of CO on Pt and is given by

$$\mathbf{F}\left(\begin{bmatrix} a \\ b \end{bmatrix}\right) = \begin{bmatrix} \frac{a}{\epsilon}(1 - a)(a - \frac{b+\beta}{\alpha}) \\ f(a) - b \end{bmatrix}, H = \begin{bmatrix} 1 & 0 \\ 0 & 0 \end{bmatrix}, \tag{2.5}$$

and

$$f(a) = \begin{cases} 0 & \text{if} \quad a < 1/3 \\ 1 - 6.75a(a-1)^2 & \text{if} \quad 1/3 \le a \le 1 \\ 1 & \text{if} \quad a > 1 \end{cases}.$$

a represents the activator concentration and b represents the inhibitor concentration. α, β, and ϵ are bifurcation parameters, with ϵ determining the difference in time scale between the slow variable b and the fast variable a. In the parameter regime of coupling-induced spatiotemporal chaos the function $\mathbf{F}$ has three relevant fixed points, a stable node $S^n = (0, 0)$, a saddle point $S^s = (\frac{\beta}{\alpha}, 0)$, and an unstable focus which must be computed numerically. Additional fixed points at $(1, 1)$ and $(\frac{1+\beta}{\alpha}, 1)$ are not relevant to the region of phase space in which chaos exists [19]. In the Bär-Eiswirth

network [Eqs. (2.1, 2.5)] a backfiring instability is reported to be the origin of spatiotemporal chaos; the traveling pulses become unstable to allow reexcitation behind the pulse to create new pulses [23, 25, 26]. In this paper we use the parameters $\alpha = 0.84$, $\beta = 0.07$, and $\epsilon = 0.12$.

The *Wacker-Schöll system* [2] describes charge transport in a simplified model of layered semiconductors and is given by

$$\mathbf{F}\left(\begin{bmatrix} a \\ b \end{bmatrix}\right) = \begin{bmatrix} \frac{b-a}{(b-a)^2+1} - \tau a \\ \alpha(j_0 - (b-a)) \end{bmatrix} \text{ and } H = \begin{bmatrix} 1 & 0 \\ 0 & d \end{bmatrix}, \tag{2.6}$$

where a represents the interface charge density, and b represents the dimensionless voltage [2]. The bifurcation parameter j_0 represents normalized external current, α determines the time scale of the system, d is an effective diffusion constant, and τ is an internal system parameter [27]. In the parameter regime of coupling-induced spatiotemporal chaos the function $\mathbf{F}$ has an unstable focus at $(\frac{j_0}{(j_0^2+1)\tau}, j_0 + \frac{j_0}{(j_0^2+1)\tau})$ and a stable limit cycle. In the Wacker-Schöll network [Eqs. (2.1, 2.6)] a Hopf bifurcation as temporal instability and a Turing bifurcation as diffusive instability cause the irregular spatiotemporal spiking pattern in spatiotemporal chaos [27]. We use the parameters $\alpha = 0.02$, $\tau = 0.05$, $j_0 = 1.21$, and $d = 8$, for which the system is near a codimension-2 Turing-Hopf bifurcation point.

All of these three dynamical systems have an excitable attractor (either node or limit cycle) such that strong enough stimuli can cause large excursions from the attractor. In the BE system and GS system the stable manifold of the saddle acts like a separatrix between excited states and states of immediate return to the attractor. In the WS-system the limit cycle is attracting but not Lyapunov stable. Its excitation cycles grow continuously with increasing perturbation from the limit cycle, and their size is large in comparison to the limit cycle already for small perturbations from the limit cycle. In all three systems, spatiotemporal chaos is introduced by diffusive coupling, and regular attractors are accessible in the case of the spatially homogeneous system. These systems differ in their coupling as the GS system has equal diffusivities, the BE system has zero diffusivity for one species, and the WS system has a diffusion-driven Turing instability. The bifurcation scenario for the uncoupled systems is also different: the GS system, Eq. (2.4), reaches the parameter regime of spatiotemporal chaos, in which there is no limit cycle present, via a subcritical Hopf bifurcation; the BE system, Eq. (2.5), reaches the parameter regime of spatiotemporal chaos, in which there is no limit cycle present, via a supercritical Hopf bifurcation that generates an unstable focus and a stable limit cycle, which disappears via a saddle loop bifurcation; in the parameter regime of

spatiotemporal chaos the WS system has a stable limit cycle that is generated via a supercritical Hopf bifurcation.

Chapter 3

Lifetime of transient spatiotemporal chaos

Earlier studies have reported that spatiotemporal chaos is transient in the two-dimensional WS model [2], the two-dimensional BE model [3], and the one- and two-dimensional GS model [4]. After a regime of sustained spatiotemporal chaos with a rapid decay of spatial correlations and a positive largest Lyapunov exponent, the systems exhibit a spontaneous, system intrinsic collapse to a regular state (Figs. 3.1a-e). Such a sudden collapse points to the coexistence of a chaotic saddle with the regular attractor(s) [18].

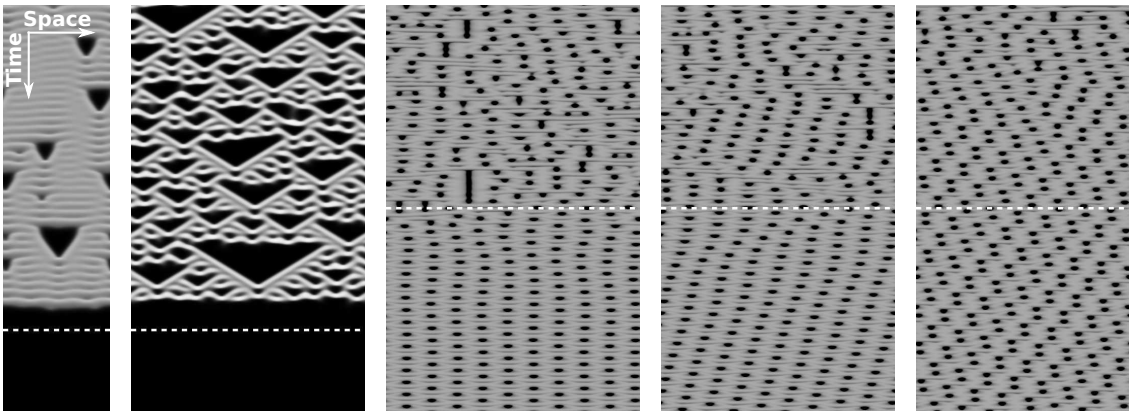

(a) (b) (c) (d) (e)

Figure 3.1. Spatiotemporal pattern of the variable a during the collapse of spatiotemporal chaos for (a) the Gray-Scott (GS) system ($\mu = 33.7$, $\Phi = 2.8$, $D = 16$, $N = 210$, and 240 time units shown), (b) the Bär-Eiswirth (BE) system ($\alpha = 0.84$, $\beta = 0.07$, $\epsilon = 0.12$, $D = 16$, $N = 200$, and 240 time units shown), and (c-e) the Wacker-Schöll (WS) system ($\alpha = 0.02$, $\tau = 0.05$, $j_0 = 1.21$, $d = 8$, $D = 0.25$, and 24000 time units shown) with different network sizes [$N = 500$ in (c), $N = 460$ in (d), $N = 420$ in (e)]. The dotted line represents the time of collapse as determined by our algorithm, with the transient lifetimes $T = 4574539$ (a), $T = 3600582$ (b), $T = 24794$ (c), $T = 491481$ (d), and $T = 32531$ (e). The pattern in (c) was observed often, with the initial wavy distortions from periodicity disappearing for large simulation times. The patterns in (d) and (e) were less common. In (d) the asymptotic state is rotated in space and time, which allows a spatial period that is a half-integer fraction of the system size. The numerical integration used periodic boundary conditions and a 4^{th} order Runge-Kutta integration method with a numerical integration timestep of $\Delta t = 0.003$ for the GS and BE systems and $\Delta t = 0.03$ for the WS system.

For the GS system and the BE system spatiotemporal chaos collapses to a spatially homogeneous stable steady state, in which the dynamics at each network node reaches the asymptotic stable

steady state S^n of the uncoupled system. This spatially homogeneous state represents the attractor on the synchronization manifold [19] in Eq. (2.1). For both systems the transient spatiotemporal chaotic pattern is characterized by an irregular distribution of black patches, in which trajectories of neighboring network nodes approach the stable steady state S^n of the homogeneous system (Fig. 3.1a and b) together. In the WS system the transient pattern is characterized by an irregular spiking (Figs. 3.1c-e). The lighter color corresponds to trajectories of neighboring network nodes being closer to the stable limit cycle of the homogeneous system, whereas the dark spots correspond to neighboring trajectories away from the stable limit cycle. Our simulations showed that the asymptotic regular state was periodic in time with various spatial shifts[1].

Transient spatiotemporal chaos is often characterized by the rate at which an ensemble of systems with different initial conditions collapses [2, 3, 18], since the transient dynamics can be very long-lived. We calculate the average lifetime $\langle T \rangle$ for transient spatiotemporal chaos explicitly for all three systems. For the Gray-Scott and the Bär-Eiswirth systems, spatiotemporal chaos only collapsed to the stable node on the synchronization manifold, and the lifetime T of transient spatiotemporal chaos is determined from

$$T = \inf_t \left\{ \max_n \left\| \mathbf{x}_n(t) - \sum_m \frac{\mathbf{x}_m(t)}{N} \right\|_\infty < 10^{-6} \right\} \tag{3.1}$$

where $\|\cdot\|_\infty$ denotes the maximum norm over the components of $\mathbf{x}$. Transient spatiotemporal chaos in the Wacker-Schöll system always collapsed into a periodic asymptotic state, and the lifetime T is determined by tracking a (finite time) maximum Lyapunov exponent [28]. When the maximum Lyapunov exponent, averaged over a gliding window of 150000 time units, drops below zero, the system is deemed to have reached a non-chaotic state starting at the beginning of the window[2].

Figures 3.2 (a)-(c) show that the average transient lifetime $\langle T \rangle$ of spatiotemporal chaos increases exponentially with the network size N for all three systems. Hence $\log \langle T \rangle$ is an extensive quantity. The rate at which $\log \langle T \rangle$ increases with N (slope of the linear fit in Fig. 3.2) depends on the boundary conditions, which is consistent with earlier studies on the Gray-Scott system [4, 29, 19]

[1]The temporal period d_t and the spatial period d_i were defined as $x(i + d_i, t + d_t) = x(i, t)$. A 2-dimensional autocorrelation analysis for the patterns in Fig. 3.1c - e) yields a temporal period of $d_t = 712.0$ and $d_i = 0.0$ for (c), $d_t = 702.2$ and $d_i = -7.4$ for (d), and $d_t = 969.8$ and $d_i = -24.5$ for (e). In comparison the period of the limit cycle for the uncoupled WS system is $d_t = 257.6$.

[2]This method determines the lifetime with sufficient accuracy, assuming that the maximum Lyapunov exponent is positive on average during the chaotic transient dynamics and zero on average during the non-chaotic dynamics, which is the case when the attractor is not a fixed point. All simulations for the Wacker-Schöll system fulfilled this criterion.

and similar to results for the two-dimensional Bär-Eiswirth system [3]. If only the larger values of N are considered the slopes are quite similar to each other and it is possible that they converge as $N \to \infty$. For example, if only data points for $\langle T \rangle > 10^5$ are fitted the slopes for periodic and no-flux boundary conditions agree to within 10% for the Gray-Scott model, which is similar to how much the slopes change when shifting the cutoff from $\langle T \rangle > 10^4$ to $\langle T \rangle > 10^5$.

This independence of the slopes from boundary conditions is supported from a qualitative argument. Exponential scaling of the average lifetime with the network size N arises if a system is comprised of weakly interacting and statistically uncorrelated units of length ξ. If P is the probability for a unit ξ to be conducive to loss of chaos at any moment of time, then spatiotemporal chaos collapses with the probability $P^{N/\xi}$, when all units are in a state conducive to collapse [18, 21]. The logarithm of the average lifetime is then $\log \langle T \rangle \sim (-N/\xi) \log P$. If a boundary condition changes the probability for collapse in one of the units to Q[3], then the logarithm of the average lifetime would be $\log \langle T \rangle \sim -\log[Q * P^{(N/\xi - 1)}] = (-N/\xi) \log P - \log(Q/P)$, which does not affect the slope. This line of reasoning is of course valid only if $Q \neq 0$[4].

Fig. 3.2 (b) also reveals that $\log \langle T \rangle$ shows significant deviation from extensivity in the Wacker-Schöll system, especially for smaller network sizes N and periodic boundary conditions. As the number of nodes increases the oscillations of $\log \langle T \rangle$ around the linear fit decrease in amplitude and match more closely the expected extensivity. One possible explanation for the deviation from extensivity is that spatial period must be an integer multiple of network size. This hypothesis is supported by the fact that the most commonly observed asymptotic pattern [2] as well as the oscillation of the deviation from extensivity of $\log \langle T \rangle$ both have a spatial period of approximately 100 nodes. For larger networks the deviation from extensivity decreases, since it becomes easier to approximate any given spatial period with an integer fraction of the network size.

An earlier study showed for the Gray-Scott system that the average lifetime is related to the number of unstable transverse modes along a typical trajectory within the synchronization manifold [19]. The number of unstable transverse modes as well as $\log \langle T \rangle$ are extensive quantities. Both quantities increase linearly with the network size for a given coupling strength D, and they both increase linearly with $1/\sqrt{D}$ for a given network size N.

[3] In the Gray-Scott system the probability for local extinction could be associated with the probability P of a unit to be conducive to collapse. Test simulations show that no-flux boundary conditions as well as shortcuts in the network change locally the probability for local extinctions.

[4] Transient spatiotemporal chaos can become asymptotic for a constant boundary condition that provides a superthreshold perturbation to the excitable reaction-diffusion network [4].

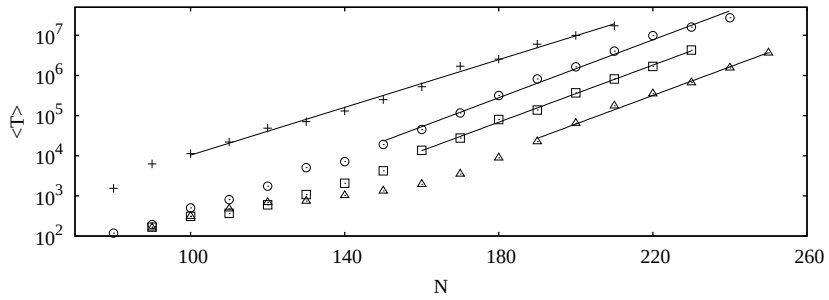

(a) Gray-Scott system

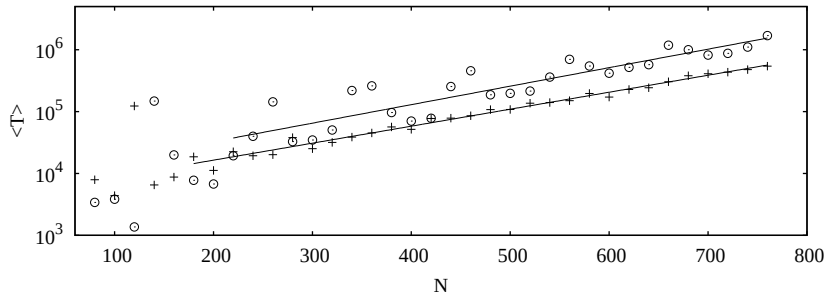

(b) Wacker-Schöll system

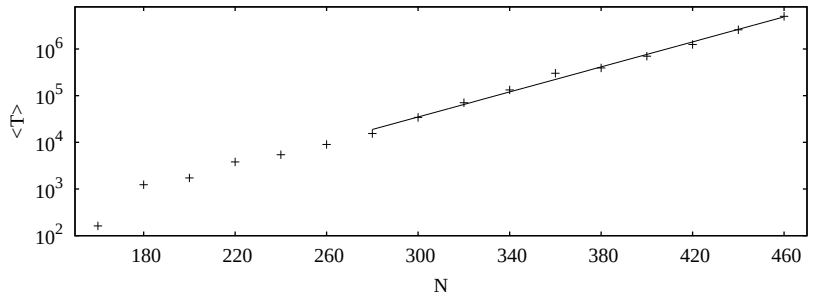

(c) Bär-Eiswirth system

Figure 3.2. Average transient lifetime $\langle T \rangle$ versus number of network nodes N for (a) the Gray-Scott system, (b) the Wacker-Schöll system, and (c) the Bär-Eiswirth system. Various boundary conditions were used, including no-flux (+), periodic (○), periodic with shortcut of length 50 (□), and periodic with shortcut of length $N/2$ (△). Each data point was determined from at least 104 random initial conditions. The error bar (1 standard deviation, not plotted here) for each data point is of the order of $\langle T \rangle$ [19]. The lines show least squares linear fits of the average transient lifetimes. The linear fit includes the range of network sizes N for which the average lifetime was consistently greater than 10^4, in order to exclude artifacts from the exaggerated significance of boundary conditions for small N. The lifetimes for small N can also be affected by the initial transient before the chaotic saddle is reached. All the other parameters and simulation procedures are the same as in Fig. 3.1.

Chapter 4
Lyapunov Exponents

4.1 Definition

Informally the first, or largest, Lyapunov exponent represents the rate at which almost any infinitesimal perturbation will grow over time, or in other words the rate at which two identical systems with nearly identical initial conditions will diverge. Suppose that $\mathbf{f}^T$ is a function mapping an initial state $\mathbf{x}(t=0)$ to the corresponding state at time $t=T$. An identical system with nearby initial conditions $\mathbf{x}(t=0)+\epsilon\mathbf{y}(t=0)$ will then evolve as

$$\mathbf{x}(t=T)+\epsilon\mathbf{y}(t=T) = \mathbf{f}^T\Big(\mathbf{x}(t=0)+\epsilon\mathbf{y}(t=0)\Big) \tag{4.1}$$

$$= \mathbf{x}(t=T)+\epsilon J^T\mathbf{y}(t=0)+O(\epsilon^2) \tag{4.2}$$

where J^T is the Jacobian of $\mathbf{f}^T$,

$$J^T \equiv \left.\frac{d\mathbf{f}^T(\mathbf{x})}{d\mathbf{x}}\right|_{\mathbf{x}(t=0)}. \tag{4.3}$$

Therefore, to first order in ϵ,

$$\mathbf{y}(t=T) = J^T\mathbf{y}(t=0). \tag{4.4}$$

The $\mathbf{y}$ are called *perturbation vectors* or *tangent vectors*. The average rate at which various $\mathbf{y}$ grow or shrink over time is given by the *Lyapunov exponents* λ_i (with $i \in \{1,\ldots,\dim\mathbf{x}\}$). The existence of the Lyapunov exponents is given by the Oseledets theorem.

Let μ be an invariant measure. The Oseledets theorem [30] states that for μ-almost all $\mathbf{x}$ and for all $\mathbf{y}\neq 0$, the limit

$$\lambda = \lim_{T\to\infty}\frac{1}{T}\log\frac{|J^T\mathbf{y}|}{|\mathbf{y}|} \tag{4.5}$$

exists and assumes up to N different values where N is the dimension of the state space. The limit value depends on $\mathbf{y}$ but not on $\mathbf{x}$ (with the caveat that the *theorem itself* applies only for almost all $\mathbf{x}$). If $\lambda_1 > \ldots > \lambda_m$ are the different possible limits then the initial perturbations leading to limits $\lambda \leq \lambda_i$ form a sequence of nested subspaces $\mathbb{R}^N = W_1 \supset \ldots \supset W_m \supset \{\emptyset\}$. In other words, the initial perturbations $\mathbf{y} \in W_i \setminus W_{i+1}$ will yield $\lambda = \lambda_i$. The Oseledets theorem actually applies to a wide class of matrix-valued functions, but when applied to the Jacobian matrix gives the Lyapunov exponents.

4.2 Computation of Lyapunov Exponents I - Theory

Since the set $W_1 \setminus W_2$ covers almost all of tangent space, it follows that almost all perturbations grow at a rate given by the largest Lyapunov exponent λ_1 (sometimes referred to as *the* Lyapunov exponent). A randomly chosen perturbation vector will therefore almost certainly expand at rate λ_1. Within the W_2 subspace, almost all perturbations are contained within $W_2 \setminus W_3$ and so will grow at a rate of λ_2. A unit disk centered at the origin in tangent space and given a random orientation will therefore almost certainly have most of its circumference contained in $W_1 \setminus W_2$ but intersect $W_2 \setminus W_3$ along a single diameter. The disk (which actually turns into an ellipse) will then grow at rate λ_1 along one axis and at rate λ_2 along the other axis, so its area will grow at rate $\lambda_1\lambda_2$. Since tangent space is linear, any shape that is coplanar with the disk will expand (or contract) in area at the same rate [31].

Consider now a set $\{\mathbf{y}_1, \ldots, \mathbf{y}_N\}$ of randomly chosen tangent vectors. Any individual vector (for example $\mathbf{y}_1$) will grow in length at rate λ_1. Any pair of vectors (for example $\mathbf{y}_1$ and $\mathbf{y}_2$) will define a parallelogram which will grow in area at rate $\lambda_1\lambda_2$. Any set of three vectors (for example $\mathbf{y}_1$, $\mathbf{y}_2$, and $\mathbf{y}_3$) will define a parallelepiped having a volume that grows at rate $\lambda_1\lambda_2\lambda_3$. In principle, observing the evolution of a set of N tangent vectors gives enough information to compute $\{\lambda_1, \ldots, \lambda_N\}$.

In practice this naïve method will lead to ill-conditioned shapes whose volumes cannot be computed in an accurate way. All of the perturbation vectors will grow exponentially at rate λ_1 and will tend to align along the direction of most rapid growth. The parallelogram defined by $\mathbf{y}_1$ and $\mathbf{y}_2$ will technically have area approaching $e^{\lambda_1\lambda_2 t}$ as time $t \to \infty$, but will rapidly be stretched into the shape of a thin needle whose area cannot be reliably computed. Numerical errors will completely swamp the λ_2 factor. The solution is to periodically normalize and orthogonalize the set of perturbation vectors using the Gram-Schmidt process. Orthonormalization causes the parallelotopes to become hypercubes of area 1 and the vectors become well conditioned from a computational perspective. The crucial property of the Gram-Schmidt transformation is that the resultant parallelotopes will have hypervolume that grows proportionately the same as it would have in the absence of the orthonormalization process.

The *Gram-Schmidt process* consists of subtracting from each vector $\mathbf{y}_m$ its projection onto each of the previous vectors $\{\mathbf{y}_n\}_{1 \le n < m}$ to produce vectors $\mathbf{v}_m$ which are all orthogonal to each other. The

$\mathbf{v}_m$ vectors are then normalized to produce orthonormal vectors $\mathbf{u}_m$:

$$\mathbf{v}_1 = \mathbf{y}_1 \tag{4.6}$$

$$\mathbf{u}_1 = \mathbf{v}_1/|\mathbf{v}_1| \tag{4.7}$$

$$\mathbf{v}_2 = \mathbf{y}_2 - \langle \mathbf{y}_2 \mid \mathbf{u}_1 \rangle \mathbf{u}_1 \tag{4.8}$$

$$\mathbf{u}_2 = \mathbf{v}_2/|\mathbf{v}_2| \tag{4.9}$$

$$\mathbf{v}_3 = \mathbf{y}_3 - \langle \mathbf{y}_3 \mid \mathbf{u}_1 \rangle \mathbf{u}_1 - \langle \mathbf{y}_3 \mid \mathbf{u}_2 \rangle \mathbf{u}_2 \tag{4.10}$$

$$\mathbf{u}_3 = \mathbf{v}_3/|\mathbf{v}_3| \tag{4.11}$$

etc.

The parallelotopes generated by the set of vectors $\{\mathbf{v}_1, \ldots, \mathbf{v}_m\}$ for $m \leq N$ have the same hypervolume as the original set of vectors $\{\mathbf{y}_1, \ldots, \mathbf{y}_m\}$, and this hypervolume is equal to $\prod_{i=1}^{m} |\mathbf{v}_i|$. The vectors $\{\mathbf{u}_1, \ldots, \mathbf{u}_m\}$, being orthonormal, generate a hypercube of hypervolume 1. This process, as stated in Eq. (4.6)-(4.11), tends to have poor numerical stability. Fortunately this is easily fixed by using what is probably the easiest numerical implementation of the above equations, in which the values of the vectors are progressively updated in-place and the updated value used for the next projection operation. See [32] for details.

The process for *computing the Lyapunov spectrum* is as follows. First, an arbitrary set of orthonormal perturbation vectors $\{\mathbf{u}_1^{(0)}, \ldots, \mathbf{u}_N^{(0)}\}$ is chosen. For each iteration k, the $\{\mathbf{u}_1^{(k-1)}, \ldots, \mathbf{u}_N^{(k-1)}\}$ vectors are evolved for a time ΔT using the linearized equations of motion to produce $\{\mathbf{y}_1^{(k)}, \ldots, \mathbf{y}_N^{(k)}\}$ which are orthonormalized using the Gram-Schmidt process to produce $\{\mathbf{v}_1^{(k)}, \ldots, \mathbf{v}_N^{(k)}\}$ and $\{\mathbf{u}_1^{(k)}, \ldots, \mathbf{u}_N^{(k)}\}$. The volume expansion during this time of each m-dimensional parallelotope is given by

$$s_m^{(k)} = \prod_{i=1}^{m} |\mathbf{v}_i^{(k)}|, \tag{4.12}$$

with $m \in \{1, \ldots, N\}$. These $\{s_1^{(k)}, \ldots, s_N^{(k)}\}$ values are stored and the $\{\mathbf{u}_1^{(k)}, \ldots, \mathbf{u}_N^{(k)}\}$ are used for the next iteration. After K iterations the total volume expansion of the m-dimensional parallelotope is given by

$$S_m^{(K)} = \prod_{k=1}^{K} s_m^{(k)}. \tag{4.13}$$

Since an m-dimensional parallelotope expands at an average rate of $\sum_{n=1}^{m} \lambda_n$, the Lyapunov exponents satisfy the relation

$$\sum_{n=1}^{m} \lambda_n = \lim_{K\to\infty} \frac{1}{K\Delta T} \ln S_m^{(K)} \tag{4.14}$$

$$= \lim_{K\to\infty} \frac{1}{K\Delta T} \sum_{k=1}^{K} \ln s_m^{(k)} \tag{4.15}$$

$$= \lim_{K\to\infty} \frac{1}{K\Delta T} \sum_{i=1}^{m} \sum_{k=1}^{K} \ln|\mathbf{v}_i^{(k)}|. \tag{4.16}$$

Therefore the individual Lyapunov exponents are given by

$$\lambda_m = \lim_{K\to\infty} \frac{1}{K\Delta T} \sum_{k=1}^{K} \ln|\mathbf{v}_i^{(k)}| \tag{4.17}$$

$$= \lim_{K\to\infty} \frac{1}{T} \sum_{k=1}^{K} \ln|\mathbf{v}_i^{(k)}|. \tag{4.18}$$

4.3 Computation of Lyapunov Exponents II - Implementation

Figure 4.1 presents a pseudocode implementation of the algorithm outlined in the previous section. It is assumed that the dynamical system is of the form $\dot{\mathbf{x}} = \mathbf{f}(\mathbf{x})$, although the same recipe should work for systems that depend explicitly on time. In the case of a reaction-diffusion network, the state vector $\mathbf{x}$ and perturbation vectors $\mathbf{y}_i$ each have one element for each variable of each node. For example, the Gray-Scott model has two variables per node, so in a network with 100 nodes the vectors would be dimension 200. The $J(t)$ are the Jacobians of $\mathbf{f}$ evaluated at $\mathbf{x}(t)$.

constant $\Delta t \leftarrow$ time step
constant $T_{rn} \leftarrow$ renormalization interval (eg. $1000\Delta t$)
constant $M \leftarrow$ number of Lyapunov exponents to compute ($\leq \dim \mathbf{x}$)
$\mathbf{x} \leftarrow$ random initial condition
$\mathbf{y}_1, \ldots, \mathbf{y}_M \leftarrow$ random orthonormal vectors
$t \leftarrow 0$ (time variable)
$a_1, \ldots, a_M \leftarrow 0$ (Lyapunov accumulators)
main loop (to be executed until satisfactory convergence has been achieved):
    iterate for time T_{rn} (i.e. for $T_{rn}/\Delta t$ steps):
        propagate $\mathbf{x}$ using $\dot{\mathbf{x}} = \mathbf{f}(\mathbf{x})$ with Runge-Kutta integration
        compute Jacobians $J(t)$, $J(t + \Delta t/2)$, $J(t + \Delta t)$
        for $i \in \{1, \ldots, M\}$:
            propagate $\mathbf{y}_i$ using $\dot{\mathbf{y}}_i = J\mathbf{y}_i$ with Runge-Kutta integration
        $t \leftarrow t + \Delta t$
    orthonormalize perturbations:
        for $i \in \{1, \ldots, M\}$:
            $a_i \leftarrow a_i + log(|\mathbf{y}_i|)$
            $\mathbf{y}_i \leftarrow \mathbf{y}_i/|\mathbf{y}_i|$
            for $j \in \{i + 1, \ldots, M\}$:
                $\mathbf{y}_j \leftarrow \mathbf{y}_j - \langle \mathbf{y}_i \mid \mathbf{y}_j \rangle \mathbf{y}_i$
    compute Lyapunov exponents:
        for $i \in \{1, \ldots, M\}$:
            $\lambda_i \leftarrow a_i/t$
    write Lyapunov exponents to output file

Figure 4.1. Pseudo-code for computation of Lyapunov exponents

Runge-Kutta integration of the $\mathbf{y}_i$ requires the Jacobians $J(t)$, $J(t + \Delta t/2)$, and $J(t + \Delta t)$. Computation of these Jacobians requires knowledge of $\mathbf{x}(t)$, $\mathbf{x}(t + \Delta t/2)$, and $\mathbf{x}(t + \Delta t)$ which in turn must be obtained using Runge-Kutta integration. Therefore, the process ultimately requires evaluation of $\mathbf{f}$ at time substeps of t, $t + \Delta t/4$, $t + \Delta t/2$, $t + 3\Delta t/4$, and $t + \Delta t$. The result of $\mathbf{x}(t + \Delta t)$ obtained in this process can be used to propagate $\mathbf{x}$. Additionally, the values of $\mathbf{x}(t + \Delta t)$ and $J(t + \Delta t)$ can be

saved and used as $\mathbf{x}(t)$ and $J(t)$ during the next iteration, although the efficiency gained by doing so may not justify the additional code complexity involved.

Code efficiency:

• In the case of a typical reaction-diffusion network the dimension of $\mathbf{x}$ may be on the order of 100-1000 or more, rendering the operation $J\mathbf{y}_i$ extremely inefficient. Fortunately, the Jacobian is separable in this case (as long as the diffusion term is linear) into reaction components that operate within each node and a diffusive component that operates between neighboring nodes. If $\mathbf{x}_1, \ldots, \mathbf{x}_N$ are the per-node components of the state variable $\mathbf{x}$ then in the case of a reaction-diffusion network $\dot{\mathbf{x}} = \mathbf{f}(\mathbf{x})$ can be written

$$\frac{d\mathbf{x}_n}{dt} = \mathbf{F}_n(\mathbf{x}_n) + D\sum_{j=1}^{N} G_{nj} H \mathbf{x}_j, \tag{4.19}$$

and if $\mathbf{y}_1, \ldots, \mathbf{y}_N$ are the per-node components of some perturbation vector $\mathbf{y}$ then $\dot{\mathbf{y}} = J\mathbf{y}$ reduces to

$$\frac{d\mathbf{y}_n}{dt} = J\mathbf{F}_n|_{\mathbf{x}_n}\,\mathbf{y}_n + D\sum_{j=1}^{N} G_{nj} H \mathbf{y}_j \tag{4.20}$$

where $J\mathbf{F}_n|_{\mathbf{x}_n}$ is the Jacobian of $\mathbf{F}_n$ evaluated at $\mathbf{x}_n$. Since $\dim \mathbf{x}_n$ is typically on the order of 2-3, the matrix multiplication is much more manageable in this form.

• Although it is technically suitable to choose completely random initial perturbations $\mathbf{y}_i$ and any initial state $\mathbf{x}$ in the attractor's basin of attraction, some strategic choices can speed up the initial convergence of the Lyapunov exponents. The best choice for the initial state $\mathbf{x}$ would be something that will quickly converge to the attractor without making any large detours. The initial perturbations $\mathbf{y}_i$ should be chosen to in some way resemble the actual Lyapunov vectors. That is to say that the first few ($\mathbf{y}_1$, $\mathbf{y}_2$, …) should be chosen such that they can be expected to grow in magnitude, or at least to not quickly decrease in magnitude. For instance, choosing Fourier modes with frequencies being assigned in order to $\mathbf{y}_1$, $\mathbf{y}_2$, … would be a good choice because these resemble the eigenvectors of the diffusion term. Delta functions would be a poor choice because they would all rapidly decrease in magnitude due to the diffusion term for quite some time before aligning themselves in a more natural direction. This would give the initial Lyapunov accumulators a large negative bias. Any initial bias will cause an error in the final result that decreases slowly (with a rate on the order of $\Theta(T^{-1})$).

• The choice of M (number of Lyapunov exponents to compute) can dramatically affect the runtime of the algorithm. For small M execution time is dominated by the Runge-Kutta integrations

which collectively have a runtime that grows as $\Theta(\Delta t^{-1} T M \dim \mathbf{x})$. For larger M the Gram-Schmidt orthonormalization dominates and runtime grows as $\Theta(T_{rn}^{-1} T M^2 \dim \mathbf{x})$. It is therefore advantageous to compute only as many Lyapunov exponents as needed. Computation of Lyapunov dimension $D_{\mathcal{L}}$ (to be discussed in the following section) requires computation of $M > D_{\mathcal{L}}$ Lyapunov exponents. A good strategy is to make an educated guess of the value of $D_{\mathcal{L}}$, choose M somewhat larger than this, run the simulation for a while to get a refined value of $D_{\mathcal{L}}$, and then use a value of M somewhat larger than that for the final (lengthy) simulation.

4.4 Lyapunov spectrum and related quantities

Measures that quantify chaotic attractors can also characterize chaotic saddles (transient spatiotemporal chaos) for large network sizes, if the lifetimes are long enough for the measures to converge. The Lyapunov spectra for the reaction-diffusion networks in Eq. (2.1) were computed numerically [31] from infinitesimal displacement vectors $\mathbf{y}_n$ about $\mathbf{x}_n$ that evolve according to $\frac{\partial \mathbf{y}_n}{\partial t} = J|_{\mathbf{x}_n} \mathbf{y}_n + D \sum_{j=1}^{N} G_{nj} H \mathbf{y}_j$, where $J|_{\mathbf{x}_n}$ is the Jacobian of $\mathbf{F}$ evaluated at $\mathbf{x}_n$. With periodic Gram-Schmidt orthonormalization of the $\mathbf{y}_n$ vectors every T_{rn} time units, and with the logarithm of the corresponding normalization coefficients being added to a running tally β_i, the (finite time) Lyapunov exponents are given by β_i/t for any time t [31]. Fourier modes were used as initial perturbations, although the choice of initial perturbation should have little effect on the final result [31]. A renormalization interval of $T_{rn} = 3$ time units was used in all cases, and simulation times varied between $2.8{\times}10^5$ and $5.6{\times}10^6$ time units. The Lyapunov spectra were robust to changes in renormalization interval and integration timestep[1]. Some of the systems collapsed into a steady or periodic state part way through the simulation[2]. If the largest Lyapunov exponent for a gliding window of length 3000 time units fell below zero, all samples after the beginning of this window were discarded. Figure 4.2 shows a typical convergence behavior of a Lyapunov exponent; it happens slowly. The convergence error was estimated as the maximum difference between the final (finite

[1] Computation of Lyapunov exponents can be sensitive to integration timestep and time between renormalization [16]. One representative system for each of the three models (Gray-Scott, Bär-Eiswirth, and Wacker-Schöll) was run with an integration timestep 5 times smaller and then with a renormalization interval 5 times shorter. In all cases the difference in either Lyapunov dimension or sum of positive Lyapunov exponents between the trial and the baseline cases was less than 1.8 times the estimated convergence error.

[2] Runs that survived for a time less than $5 \times 10^6 \Delta t$ were discarded under the assumption that not enough data would be available to get a reliable value for the Lyapunov exponents. Additionally, each system is run to time $10000\Delta t$ before perturbation vectors are followed to minimize the significance of the initial period before the chaotic saddle has been reached, and the perturbation vector data gathered in the first 4500 time units was discarded in order to allow the vectors to align in a natural way.

time) Lyapunov exponent and any intermediate value from the second half of the simulation.

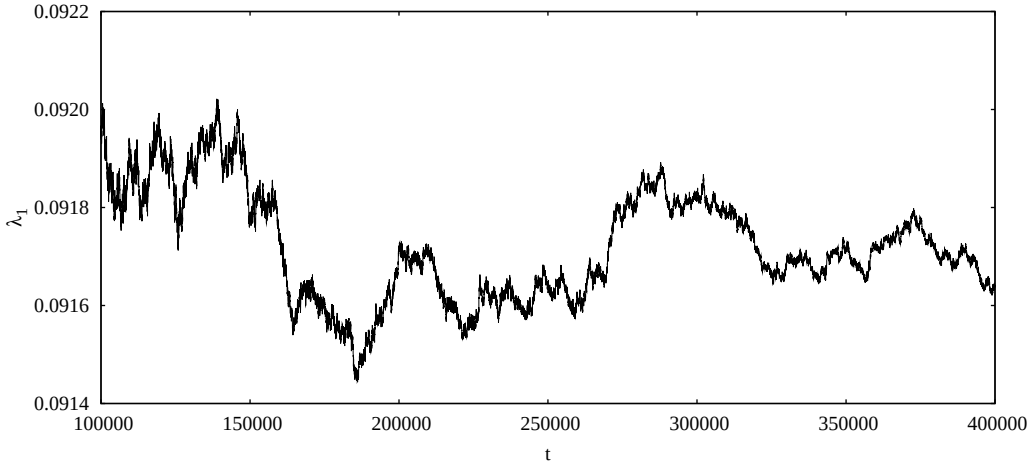

Figure 4.2. Convergence behavior of the largest (finite time) Lyapunov exponent λ_1 for the Gray-Scott system with simulation time t. This convergence behavior is typical for Lyapunov exponents in all three models. The error is estimated by computing the maximum difference between the final value and any value from the second half of the simulation.

Spatiotemporal chaos is said to be extensive if the spectrum of Lyapunov exponents λ_i converges to a function $f(i/N)$ that is intensive. This implies that the attractor dimension increases in proportion to the system size N and that a dimension density exists [12]. We will show that transient spatiotemporal chaos also fulfills these criteria for all three models.

Figure 4.3 shows a *single Lyapunov exponent* λ_i for each network size N, with the index $i = N/20\sqrt{D} + 1$ scaled in proportion to the network size N. $\lambda_{N/(20\sqrt{D})+1}$ converges with N in good approximation. This behavior is consistent with the spectrum of Lyapunov exponents converging to a function that is intensive, and with the existence of a Lyapunov spectrum density. Qualitatively similar convergence behavior was found for the Lyapunov spectrum in the Bär-Eiswirth model and in the Wacker-Schöll model.

The *Lyapunov dimension* ($D_{\mathcal{L}}$) is conjectured to be equal to the information dimension for typical attractors [33]; it is defined as

$$D_{\mathcal{L}} = j + \frac{\lambda_1 + \ldots + \lambda_j}{|\lambda_{j+1}|}, \tag{4.21}$$

where j is the largest integer for which $\sum_{i=1}^{j} \lambda_i > 0$. For chaotic saddles the information dimension has a correction term proportional to the escape rate, which is negligible for large enough system

sizes such as those considered in this paper [34].

Figure 4.4(a) shows that the Lyapunov dimension $D_{\mathcal{L}}$ increases linearly with the network size N for all three reaction-diffusion network models with varying system parameters. The deviation of the $D_{\mathcal{L}}$-values from linearity was small for all systems studied; a representative example for the Gray-Scott system is given in fig. 4.4(b). These findings indicate that $D_{\mathcal{L}}$ is an extensive quantity during the transient phase of spatiotemporal chaos. Extensive transient spatiotemporal chaos in these models was also found for various boundary conditions, including periodic and no-flux boundary conditions as well as periodic with the presence of shortcuts in the network. The results are summarized in Table 4.1.

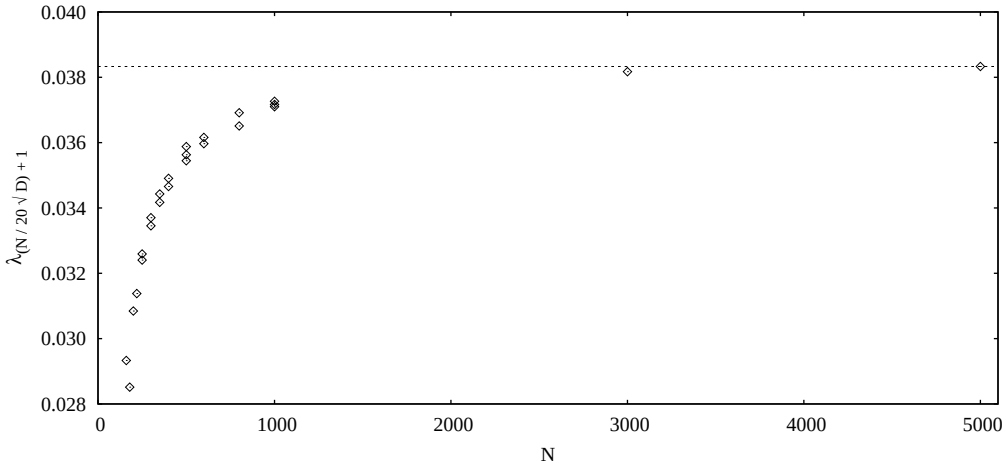

Figure 4.3. The scaled index Lyapunov exponent $\lambda_{N/(20\sqrt{D})+1}$ vs. network size N for the Gray-Scott system. Lyapunov exponents are indexed starting from λ_1, and linear interpolation is used in cases where the index $i = N/20\sqrt{D} + 1$ is not an integer. The multiple data points for certain values of N correspond to different initial conditions and are close together. All the other parameters are the same as in Fig. 3.1(a). The dotted line is included as a visual aid.

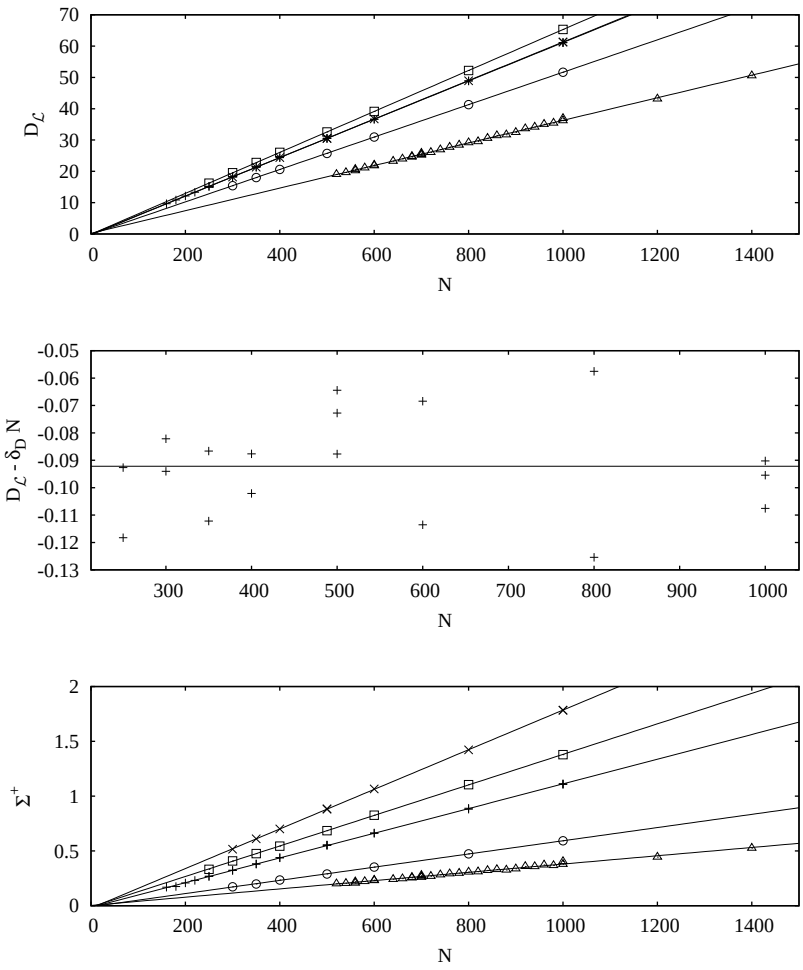

Figure 4.4. Various extensive quantities vs. network size N: (a) Lyapunov dimension $D_{\mathcal{L}}$ versus network size N for five systems with periodic boundary conditions: Bär-Eiswirth model with $\alpha = 0.84$, $\beta = 0.07$, $\epsilon = 0.12$, $D = 16$ (×), Gray-Scott model ($\phi = 2.8$, $D = 16$) with $\mu = 33.5$ (□), $\mu = 33.7$ (+), $\mu = 33.9$ (○), and Wacker-Schöll model with $\alpha = 0.02$, $\tau = 0.05$, $j_0 = 1.21$, $d = 8$, $D = 0.25$ (△). The Lyapunov dimension for the Bär-Eiswirth model (×) and the Gray-Scott model ($\mu = 33.7$, +) have very similar values, making them hard to distinguish in the graph, although their Lyapunov spectra are different. The full lines correspond to a least square linear fit of the corresponding data points. The error for each data point, not plotted in the figure, was estimated by computing the maximum difference between the final value of $D_{\mathcal{L}}$ and any intermediate value from the second half of the simulation; errors were smaller than 2.5% of the data point values and typically less than 0.3% for Gray-Scott and Bär-Eiswirth systems. (b) Deviation of $D_{\mathcal{L}}$-values from the linear fit in (a) for the Gray-Scott system with $\mu = 33.7$. For this system $D_{\mathcal{L}}$ was calculated for different initial conditions for each network size N to estimate the convergence behavior. These data points were plotted in both figures, (a) and (b), but they are too close to be distinguished in (a). The horizontal line represents the y-intercept of the linear fit, which was not subtracted when plotting deviation from the linear trend. (c) Sum of positive Lyapunov exponents Σ^+ versus network size N for the same systems as in (a). The values for the Wacker-Schöll system have been multiplied by 20 to improve clarity.

Table 4.1. Summary of Lyapunov dimension $D_{\mathcal{L}}$ and sum of positive Lyapunov exponents $\sum^+$ for the Bär-Eiswirth (BE) model ($\alpha = 0.84$, $\beta = 0.07$, $\epsilon = 0.12$), the Gray-Scott (GS) model ($\mu \in \{33.5, 33.7, 33.9\}$, $\Phi = 2.8$), and the Wacker-Schöll (WS) model ($\alpha = 0.02$, $\tau = 0.05$, $j_0 = 1.21$, $d = 8$) for different system parameters and different boundary conditions. A least square linear fit was made for $D_{\mathcal{L}}$ and Σ^+ versus network size N, and a least square linear fit was made for $D_{\mathcal{L}}$ and Σ^+ versus $1/\sqrt{D}$ with coupling parameter D. A least square constant fit was done for $D_{\mathcal{L}}$ and Σ^+ for fixed effective system sizes $N/\sqrt{D}$ = constant.

System	Fixed Parameter	Boundary Condition	Linear fit for $D_{\mathcal{L}}$	RMS error of fit	Linear fit for Σ^+	RMS error of fit
BE	N=500	Periodic	$-1.499 + 128.9/\sqrt{D}$	0.2421	$-0.06705 + 3.818/\sqrt{D}$	0.007420
BE	D=16	Periodic	$-0.2175 + 0.06151N$	0.03850	$-0.02241 + 0.001807N$	0.002020
BE	$\frac{N}{\sqrt{D}}$=250	Periodic	62.15	0.7946	1.813	0.02769
WS	D=0.25	No-flux	$0.9767 + 0.03539N$	0.3115	$0.001189 + 1.791 \times 10^{-5}N$	0.0003796
WS	D=0.25	Periodic	$0.2272 + 0.03606N$	0.2304	$0.0001183 + 1.890 \times 10^{-5}N$	0.0003587
WS	$\frac{N}{\sqrt{D}}$=2000	Periodic	36.99	0.6054	0.02022	0.001271
GS, μ=33.5	N=500	Periodic	$-0.05447 + 130.5/\sqrt{D}$	0.01766	$-0.03049 + 2.872/\sqrt{D}$	0.004593
GS, μ=33.5	D=16	Periodic	$-0.1074 + 0.06540N$	0.02012	$-0.01160 + 0.001393N$	0.002511
GS, μ=33.5	$\frac{N}{\sqrt{D}}$=250	Periodic	65.05	0.2733	1.450	0.07389
GS, μ=33.7	N=500	Periodic	$-0.07992 + 122.4/\sqrt{D}$	0.01723	$-0.01816 + 2.281/\sqrt{D}$	0.001831
GS, μ=33.7	D=16	Periodic	$-0.1148 + 0.06125N$	0.02296	$-0.01462 + 0.001126N$	0.003871
GS, μ=33.7	$\frac{N}{\sqrt{D}}$=250	Periodic	61.11	0.03848	1.138	0.04028
GS, μ=33.7	D=16	No-flux	$0.3643 + 0.06126N$	0.007197	$0.01095 + 0.001122N$	0.001092
GS, μ=33.7	D=16	Shortcut, $k = 50$	$-1.528 + 0.06121N$	0.02385	$-0.03057 + 0.001117N$	0.001562
GS, μ=33.7	D=16	Shortcut, $k = N/2$	$-1.233 + 0.06124N$	0.02963	$-0.04299 + 0.001118N$	0.004419
GS, μ=33.9	N=500	Periodic	$-0.08079 + 103.3/\sqrt{D}$	0.03807	$-0.01055 + 1.203/\sqrt{D}$	0.002227
GS, μ=33.9	D=16	Periodic	$-0.1022 + 0.05175N$	0.01903	$-0.009298 + 0.0006021N$	0.001796
GS, μ=33.9	$\frac{N}{\sqrt{D}}$=250	Periodic	51.63	0.07226	0.5970	0.01081

The *sum of positive Lyapunov exponents* ($\sum^+$) represents an upper bound for the Kolmogorov-Sinai entropy [33]. For chaotic saddles this upper bound can be refined by subtracting the escape rate [35]. Figure 4.4(c) and Table 4.1 show that $\sum^+$ is an extensive quantity for all three models with varying system parameters and boundary conditions.

The Gray-Scott system was simulated for four different boundary conditions: periodic, no-flux, periodic with an added shortcut in the network of length $k = 50$ ($k << N$), and with an added shortcut of length $k = N/2$. Table 4.1 shows that the rate at which the Lyapunov dimension $D_{\mathcal{L}}$ (and also $\sum^+$) increases with the network size N is rather independent of these boundary conditions, but their Y-intercepts are significantly different for different boundary conditions. This is consistent with the finding in Sect. III for the rate at which the average transient lifetimes $\langle T \rangle$ increase with N. For a fixed network size, Fig. 3.2 and Table 4.1 reveal that $\langle T \rangle$, $D_{\mathcal{L}}$, and $\sum^+$ are largest for no-flux boundary conditions, second largest for periodic boundary conditions, and third largest for the presence of a shortcut in the network. There are, however, differences in the rankings for $\langle T \rangle$, $D_{\mathcal{L}}$, and $\sum^+$ for the two different types of shortcut length.

In the following we present a qualitative argument for why the linear fit of Lyapunov dimension $D_{\mathcal{L}}$ vs. network size N has nearly zero Y-intercept for all systems with periodic boundary conditions, as seen from Fig. 4.4(a) and Table 4.1. If we assume that subsystems in reaction-diffusion networks do not interact across large distances, the Lyapunov dimension should not be affected by transformations that alter the global topology but conserve the local network structure and the total number of nodes. Figure 4.5 shows such a transformation that turns two networks of N nodes into one network of $2N$ nodes. Since the Lyapunov dimension is additive among non-connected systems we expect that $D_{\mathcal{L}}(2N) = 2D_{\mathcal{L}}(N)$. Together with the linear ansatz, $D_{\mathcal{L}} = aN + b$, it follows that $b = 0$. This indicates that the Lyapunov dimension for very large system sizes and long simulation times follow a linear law with zero intercept. For systems with no-flux boundary conditions this line of reasoning is not valid since two such systems cannot be combined into one without changing the local structure (i.e. two of the no-flux boundaries would have to be removed).

For a ring network we also vary the coupling parameter D while keeping the network size N fixed. We find that the Lyapunov dimension $D_{\mathcal{L}}$ as well as the sum of positive Lyapunov exponents $\sum^+$ increase linearly with $1/\sqrt{D}$ for all three reaction-diffusion networks and various system parameters (Table 4.1).

The general characteristics of the reaction-diffusion networks in Eq. (2.1) is conserved if N and

D vary such that $N/\sqrt{D}$ is fixed (Sect.II). Table 4.1 shows that in this case $D_{\mathcal{L}}$ as well as $\sum^+$ are constant for a wide range of N- and D-values. Figure 4.6 also confirms for the Bär-Eiswirth model that the Lyapunov dimension is constant over a range of coupling parameters D, when $N/\sqrt{D}$ is fixed. Significant deviations from a constant Lyapunov dimension exist for small values of D, where the network model deviates significantly from the continuum model. $D_{\mathcal{L}}$ was about 58 percent higher when $D = 0.3136$ compared to the regime of constant dimension [Fig. (4.6)]. Two simulations with different initial conditions were made for each of the coupling parameters, $D = 4$ and $D = 16$, and the results are close enough that the difference between the two simulations is difficult to see on the graph in Fig. (4.6). For the Gray-Scott systems (with three different system parameters, Table 4.1) the Lyapunov dimension was constant (within 1.4%) for coupling parameters D even down to $D = 1$, which is close to the point where the system can no longer support chaos ($D \approx 0.7$). The Wacker-Schöll system had a variation in $D_{\mathcal{L}}$ of about 4% and a variation in Σ^+ of about 19% over the range of coupling parameters, $0.04 \leq D \leq 0.25$, that are close to the value for which the system can no longer support chaos. The qualitative behavior of Σ^+ was similar to that of $D_{\mathcal{L}}$, but in general had larger relative variations.

The qualitative argument for why the range of D for which $D_{\mathcal{L}}$ and $\sum^+$ are constant is bounded from below for all three reaction-diffusion networks follows from the excitability property. If D is low enough, the coupling term in Eq. (2.1) can no longer provide superthreshold perturbations to perturb the system away from the stable rest state and sustain spatiotemporal chaos.

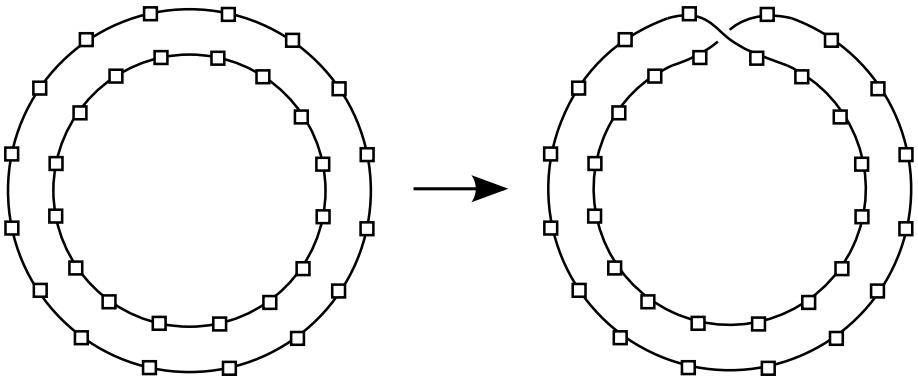

Figure 4.5. A transformation from two ring networks of N nodes into one network of $2N$ nodes, without changing the local network structure or the total number of nodes.

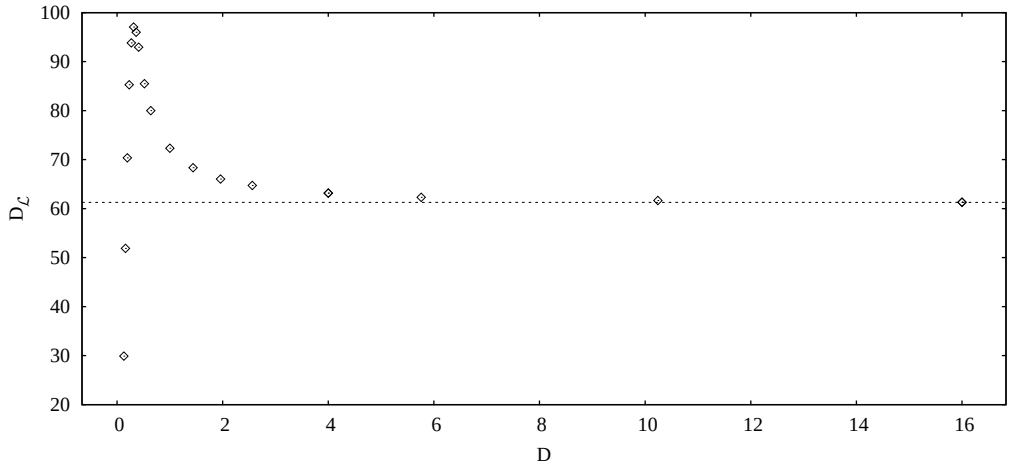

Figure 4.6. Lyapunov dimension $D_{\mathcal{L}}$ vs. coupling constant D for the Bär-Eiswirth ring network ($\alpha = 0.84$, $\beta = 0.07$, and $\epsilon = 0.12$). The effective system size was held constant by varying the number of nodes N according to $N/\sqrt{D} = 250$. This system had particularly large deviations from constant $D_{\mathcal{L}}$ for small D. The dotted line is included as a visual aid.

Chapter 5

Combining lifetime and Lyapunov quantities

5.1 Chaotic saddle as quasi-attractor

Hunt, Ott, and Yorke have conjectured a formula for computing the dimension of the stable and unstable manifolds (D_s, D_u) of a chaotic saddle based upon the Lyapunov spectrum and escape rate [34]. In the case of very low escape rate their formula reduces to [18]

$$\begin{aligned} D_s &= 2N - \frac{\kappa}{\lambda_1} \text{ and} \\ D_u &= D_{\mathcal{L}} - \frac{\kappa}{|\lambda_{j+1}|}, \end{aligned} \tag{5.1}$$

where $2N$ is the dimension of the phase space, $\kappa = \langle T \rangle^{-1}$ is the escape rate, λ_1 is the largest Lyapunov exponent, $D_{\mathcal{L}}$ is the Lyapunov dimension, and j is the largest integer for which $\sum_{i=1}^{j} \lambda_i > 0$.

When the lifetime is long enough that computation of the Lyapunov spectrum is feasible, the stable manifold has dimension nearly equal to that of the entire phase space and the unstable manifold has dimension nearly equal to the Lyapunov dimension of the saddle. For instance in the case of the Wacker-Schöll ring network ($\alpha = 0.02$, $\tau = 0.05$, $j_0 = 1.21$, $d = 8$, $D = 0.25$) with $N = 600$ nodes, $\langle T \rangle = 4.19 \times 10^5$, $\lambda_1 = 0.00276$, $j = 22$, and with $\lambda_{23} = -0.00321$, the stable and unstable manifold of the chaotic saddle have dimensions

$$\begin{aligned} D_s &= 2N - 0.000865, \\ D_u &= D_{\mathcal{L}} - 0.000744, \text{ with } D_{\mathcal{L}} = 22.02 \pm 0.14. \end{aligned}$$

The uncertainty due to convergence of $D_{\mathcal{L}}$ is approximately 0.14, which is more than two orders of magnitude larger than the corrections. As $N \to \infty$ we have $\kappa \to 0$ and so $D_s \to 2N$ and $D_u \to D_{\mathcal{L}}$. For the Bär-Eiswirth ring network ($\alpha = 0.84$, $\beta = 0.07$, $\epsilon = 0.12$, $D = 16$) with $N = 400$ nodes , $\langle T \rangle = 7.01 \times 10^5$, $\lambda_1 = 0.131$, $j = 24$, and with $\lambda_{25} = -0.129$, the dimension of the stable and unstable manifold are

$$\begin{aligned} D_s &= 2N - 0.0000109, \\ D_u &= D_{\mathcal{L}} - 0.0000111, \text{ with } D_{\mathcal{L}} = 24.386 \pm 0.053. \end{aligned}$$

For the Gray-Scott ring network ($\mu = 33.7$, $\Phi = 2.8$, $D = 16$) with $N = 200$ nodes , $\langle T \rangle = 1.64 \times 10^6$,

$\lambda_1 = 0.0792$, $j = 12$, and with $\lambda_{13} = -0.107$, the dimension of the stable and unstable manifold are

$$D_s = 2N - 0.00000770,$$
$$D_u = D_{\mathcal{L}} - 0.00000568, \text{ with } D_{\mathcal{L}} = 12.124 \pm 0.012.$$

Following the argumentation by Tel and Lai [18], the chaotic saddle behaves like a quasi-attractor for all three models, since the unstable manifold of the chaotic saddle has nearly the same dimension as the saddle ($D_u \approx D_{\mathcal{L}}$), and since the stable manifold is nearly space-filling, i.e. the stable manifold nearly forms a basin of attraction for the quasi-attractor. In addition, the dimension of the chaotic saddle is very close to the dimension of an attractor with the same Lyapunov spectrum [18].

5.2 Intensive quantities

Densities can be defined from the extensive quantities $D_{\mathcal{L}}$ and $\log\langle T\rangle$. The *(Lyapunov) dimension density* (δ_D) is given by

$$\delta_D = \lim_{N\to\infty} N^{-1} D_{\mathcal{L}}, \tag{5.2}$$

which describes the number of active degrees of freedom per unit volume [14]. Likewise, *the log-lifetime density* δ_T is defined as

$$\delta_T = \lim_{N\to\infty} N^{-1} \ln\langle T\rangle. \tag{5.3}$$

From Sect. V it follows that the *dimension density of the stable manifold of the chaotic saddle* [18], $\delta_s = D_s/N$, is about $d = 2$ for all our model systems, since $D_s \approx 2N$ in Eq. (5.1) with $2N$ the dimension of the phase space and with $d = 2$ the dimension of the uncoupled dynamical system in Eq. (2.1). The *dimension density of the unstable manifold of the chaotic saddle,* $\delta_u = D_u/N$, is about $\delta_u = \delta_D$ since $D_u \approx D_{\mathcal{L}}$ for all our model systems. Due to these similarities we focus on the dimension of the chaotic saddle (δ_D) in the following.

Table 5.1 shows that the dimension densities are rather small for the chaotic saddle in all model systems, reflecting a low degree of freedom per network node. This is consistent with an earlier study by Strain and Greenside [3] for the Bär-Eiswirth model in two spatial dimensions. Table 5.1 also reveals that the dimension density δ_D does not depend on the boundary condition. The log-lifetime density δ_T is also rather low for all model systems with a dependence on boundary conditions that appears to decrease as $N \to \infty$.

Table 5.1. Log-lifetime density δ_T and Lyapunov dimension density δ_D for the Bär-Eiswirth (BE) model ($\alpha = 0.84$, $\beta = 0.07$, $\epsilon = 0.12$, $D = 16$), the Gray-Scott (GS) model ($\mu = 33.7$, $\Phi = 2.8$, $D = 16$), and the Wacker-Schöll (WS) model ($\alpha = 0.02$, $\tau = 0.05$, $j_0 = 1.21$, $d = 8$, $D = 0.25$) for different boundary conditions. Points were only considered for the linear fit if they were within the range of N for which $\langle T \rangle$ was consistently larger than the cutoff value.

System	Cutoff	Boundary Condition	δ_D	δ_T	$\sigma = \delta_T/\delta_D$
BE	10^4	Periodic	0.0615	0.0309	0.502
GS	10^4	No-flux	0.0613	0.0685	1.12
GS	10^4	Periodic	0.0613	0.0831	1.36
GS	10^4	Shortcut, $L = 50$	0.0612	0.0818	1.34
GS	10^4	Shortcut, $L = N/2$	0.0612	0.0820	1.34
WS	10^4	No-flux	0.0354	0.00632	0.179
WS	10^4	Periodic	0.0361	0.00689	0.191
BE	10^5	Periodic	0.0615	0.0292	0.474
GS	10^5	No-flux	0.0613	0.0718	1.17
GS	10^5	Periodic	0.0613	0.0788	1.29
GS	10^5	Shortcut, $L = 50$	0.0612	0.0839	1.37
GS	10^5	Shortcut, $L = N/2$	0.0612	0.0757	1.24
WS	10^5	No-flux	0.0354	0.00613	0.173
WS	10^5	Periodic	0.0361	0.00576	0.160

We qualitatively relate the densities to properties of the weakly coupled subsystems in extensive transient spatiotemporal chaos. The exponential scaling of the average lifetime with the network size (Type-II supertransients, [18]) can be qualitatively explained by assuming weakly interacting correlated units of length ξ, with ξ approximately equal to the correlation length of the system. At any moment of time each of these units is conducive to loss of chaos with probability P. Spatiotemporal chaos collapses when all units are in such a conducive state [18], which happens with probability $P^{N/\xi}$. The lifetime takes the form

$$\langle T \rangle \sim P^{-N/\xi} = e^{-(\ln P)\frac{N}{\xi}}. \tag{5.4}$$

With Eq. (5.3) follows

$$\delta_T = \frac{-\ln P}{\xi}. \tag{5.5}$$

for finite N. δ_T can now be interpreted as having units of number of coin tosses per unit length ξ. δ_T has the advantage of being a single computable quantity [from Eq. (5.3)], whereas the intuitive argument uses two quantities, ξ and P, both of which are open to interpretation. The ratio (σ) of these densities

$$\sigma = \delta_T / \delta_D \tag{5.6}$$

defines an intensive quantity that depends neither on the network size N nor on the coupling constant D, since $\langle T \rangle$ as well as $D_{\mathcal{L}}$ is proportional to $N/\sqrt{D}$ from Sect. IV. If δ_T is interpreted as having units of number of coin tosses per unit length and δ_D is interpreted as being the number of active degrees of freedom per unit length, then σ has units of number of coin tosses per active degree of freedom. This quantity is significant because it is intensive and independent of the coupling strength, and thus suggests that transient spatiotemporal chaos in reaction-diffusion networks with homogeneous network structure can be understood from its local dynamics.

Combining Eqs. (5.3) and (5.6) to

$$\langle T \rangle^{-1} = e^{-\sigma D_{\mathcal{L}}} = (e^{-\sigma})^{D_{\mathcal{L}}} \tag{5.7}$$

leads to an intuitive argument for the escape rate from the chaotic saddle in the limit $N \to \infty$, if we assume that σ is given. Equation (5.7) can be interpreted as the volume of a hypercube of width $e^{-\sigma}$, if we ignore that the dimension of the chaotic saddle is fractal, and if we ignore that $D_{\mathcal{L}}$ is only approximately the fractal dimension. This hypercube can be considered as a hole in the

chaotic saddle through which a trajectory can escape into a nonchaotic state. Larger systems have an attractor which resembles a set product of smaller systems, and the escape hole resembles a set product of identical low dimensional boxes with edges that have a geometric mean of $e^{-\sigma}$.

Chapter 6
Conclusions

A systematic study reveals that transient spatiotemporal chaos is extensive in three reaction-diffusion networks with various boundary conditions. The Lyapunov dimension, the sum of positive Lyapunov exponents, and the logarithm of the transient lifetime grow linearly with system size. This indicates that even in the case of transient dynamics the larger systems act as if they were comprised of weakly interacting and statistically similar subsystems, with no new collective phenomena arising when such subsystems connect together. This might open up the possibility for modeling transient spatiotemporal chaos with statistical mechanics [17].

The effective system size for a network with N nodes and coupling parameter D is determined by $N/\sqrt{D}$. For a wide variety of coupling parameters and network sizes the number of active degrees of freedom (expressed in the Lyapunov dimension) stays constant as long as the effective system size is fixed. An upper bound for the entropy (expressed by the sum of positive Lyapunov exponents) is also constant for fixed effective system size. Unless the coupling parameter D is sufficiently small, the network model approaches the continuum model.

The spontaneous collapse of spatiotemporal chaos points to the coexistence of a chaotic saddle with the regular attractor(s). Applying the dimension formulas of Hunt, Ott and Yorke [34], we find for all three models that the dimension of the unstable manifold of the chaotic saddle is nearly the dimension of the chaotic saddle, and the stable manifold of the chaotic saddle is nearly space-filling. Thus the chaotic saddle behaves like a quasi-attractor according to Tél and Lai [18].

For extensive transient spatiotemporal chaos a dimension density and a log-lifetime density can be defined. A qualitative argument relates the escape rate from the chaotic saddle to a hole through which a trajectory can escape into a non-chaotic state. This hole has the form of a hyperrectangle; its dimension is the Lyapunov dimension, and its width is determined by the ratio of log-lifetime density and dimension density.

The boundary conditions seemingly do not affect the dimension density and the log-lifetime density, but do affect the x-intercept of the graphs of Lyapunov dimension versus network size and log-lifetime versus network size. It would be interesting to study whether the choice of boundary conditions shifts both the Lyapunov dimension and the log-lifetime graphs by the same number of nodes. In this case boundary conditions would change the effective network size. Unfortunately, since the computation time required to compute average lifetime grows exponentially with the net-

work size, the range of network sizes that are currently computationally accessible by supercomputers is not sufficient to determine the offset for different boundary conditions accurately enough because the slopes converge slowly.

Chapter 7
Outview

In the course of my research I have identified many potential directions that are worthy of further study. As far as I know these are all open problems, although I have not done an extensive search of the literature for any of them. These areas can for the most part be divided into the categories of phenomena relating to large networks and those relating to small networks.

Large networks: The evidence provided in this paper, as well as that provided by numerous other researchers certainly supports the conclusion that reaction-diffusion networks (in either one or two dimensional configurations) are extensive. It is apparent that the qualitative dynamics of any local area are not affected in any observable way by distant parts of the network. It is therefore reasonable to hope that certain quantities, such as Lyapunov dimension density or log-lifetime density, should be computable through observation of only a small part of a network. That such techniques have not been developed is however probably not due to a lack of trying. I suggest that a possible first step forward would be to seek out an understanding of the shape of a chaotic attractor in terms of local regions of a network. Disjoint networks will collectively have an attractor which is just a Cartesian product of the attractors of the individual sub-networks. Large networks, in many ways qualitatively resembling collections of smaller networks (as described in the discussion surrounding Fig. 4.5), should have an attractor that is *"almost a Cartesian product"* of attractors for smaller systems. It is not clear to me what exactly "almost a Cartesian product" is supposed to mean. The difference between the two systems in Fig. 4.5 is in the overall topology of the network and this is what defines the difference between a Cartesian product and an "almost Cartesian product." Once this difference is understood it may be possible to find a natural way of confining perturbation vectors to a localized region of a network in order to compute localized Lyapunov exponents. The first Lyapunov vector tends to be confined into a localized packet anyway [36], although the packet does drift around.

It seems clear to me, although I haven't verified it, that the concept of extensivity can be extended to account for boundary conditions and other exotic topologies. In this paper it was shown that the graph of Lyapunov dimension vs. number of nodes has a y-intercept that depends on boundary conditions and a slope that does not depend on boundary conditions. This can be interpreted to mean that ordinary parts of the network (i.e. parts that are just a simple linear chain of nodes) have a certain Lyapunov dimension density and that the exceptional parts of the network (i.e. the bound-

ary nodes) alter the Lyapunov dimension by a certain constant value. This should be true of more exotic topologies as well: nodes connecting three or four linear chains together should also have a constant impact on Lyapunov dimension. It would therefore be possible to build a sort of dictionary of network connections giving the Lyapunov dimension associated with each linkage. As long as each of these connections are far enough apart from each other the Lyapunov dimension should just be δ_D times the number of nodes plus the values from the dictionary. Networks where the reaction parameters (eg. ϕ and μ in the case of the Gray-Scott model) are not constant can be treated in the same way. In this case δ_D becomes a function of the reaction parameters. If the parameters change gradually, then this is all that is needed. If there is a sharp change in parameter from one node to the next, then that is just another thing that is to be added to the dictionary. Similar arguments apply for $\log \langle T \rangle$.

Small networks: Although reaction-diffusion networks are expected to show extensive behavior in the limit $N \to \infty$, the same cannot be said for very small networks. In the extreme case of $N = 1$, chaos is not even possible in a continuous-time two variable system. So how about networks that are large enough to display chaos, but are still relatively small? Fishman and Egolf demonstrated that the complex Ginzburg-Landau system in fact shows significant deviations from extensivity for small networks [17]. The deviations take an exponentially decaying sinusoidal form. The authors conjecture that this is due to the chaos being made of an integer number of "building blocks." It would be interesting to see whether the three systems in the present paper show the same behavior for small network sizes. Computation of Lyapunov exponents in this regime is hindered by the fact that the lifetime of the transient chaotic interval is rather short. It is possible however to modify the Lyapunov exponent computation algorithm to avoid this problem. As the simulation is being run, a look-ahead is done. Whenever the look-ahead determines that chaos is destined to end within a certain time, a tiny random perturbation is added to the system. Different perturbations are tried until one is found that prevents the loss of chaos. Looking further into the future allows usage of a smaller perturbation. If the perturbations are done in the subspace of Lyapunov vectors corresponding to positive Lyapunov exponents, a claim can be made that there was an initial condition that would have led to the perturbed state. Basically, the trajectory that ends up being followed is very close to what would be seen if the initial condition was exactly on the chaotic saddle (i.e. if a trajectory had been chosen that stays on the chaotic saddle for an infinite amount of time).

The complex Ginzburg-Landau system used by Fishman and Egolf is given by [17]

$$\frac{d}{dt}A = A + (1 + ic_1)\frac{d^2}{dx^2}A - (1 - ic_3)|A|^2 A, \tag{7.1}$$

where A is a complex number. This system is unique in that the dynamical equations have a U(1) gauge invariance, which is to say that there is symmetry under multiplication by a complex number of unit magnitude. The significance of this is that there is an opportunity to introduce a rather exotic boundary condition. With periodic boundary conditions, a non-local "twist" can be introduced into the system so that it resembles a sort of Möbius strip. This is accomplished by introducing a multiplication by a complex number of unit magnitude when the $\frac{d^2}{dx^2}$ operator crosses a certain boundary. If the network is thought of as a torus, with the large circumference corresponding to the x variable and the small circumference corresponding to the phase of the A variable, then this is equivalent to breaking the torus, introducing a twist, and then reconnecting it. The twist is not visible on a local scale, only on a global scale. By the logic surrounding the discussion of Fig. 4.5, this should not make a qualitative difference for very large networks. For small networks on the other hand it does make a difference. I had conjectured that Fishman's building blocks should need to attach to each other in some way, and introducing this twist would make them not fit together in the same way, possibly altering the phase of their deviations from extensivity. The result I had found was that the deviations did not alter in phase, but rather altered in magnitude. The complex Ginzburg-Landau system can be extended by using quaternions instead of complex numbers. In this case there is a $SU(2)$ gauge invariance (i.e. symmetry under multiplication by a unit quaternion) and therefore a much richer set of non-local "twists" that can be used. A preliminary low-accuracy computation seemed to show that the quaternion Ginzburg-Landau system, although qualitatively similar to the complex Ginzburg-Landau, in fact had no deviations from extensivity.

A line of research that I am currently pursuing involves the scrambling of information as it travels through a reaction-diffusion network. It is clear that distant areas of a network do not affect each other in a qualitatively observable way, but I am not aware of any attempt to quantify the length scales involved in this decoupling. My main line of attack involves statistical observations of nodes at varying distances from network boundaries, specifically averages over time of various parameters. My experiments have yielded deviations of the time averages of various parameters near boundaries as compared to corresponding averages far away from the boundaries. Some of these deviations showed a clear exponential decay as a function of distance from network boundaries.

The coefficient of this exponential decay defines a novel length scale which determines the distance over which parts of the network are decoupled from one another.

Bibliography

[1] D. Stahlke and R. Wackerbauer. *Phys. Rev. E*, 80(5):056211, Nov 2009.

[2] A. Wacker, S. Bose, and E. Schöll. *Europhys. Lett.*, 31(5-6):257, 1995.

[3] M. Strain and H. Greenside. *Physical Review Letters*, 80(11):2306–2309, 1998.

[4] R. Wackerbauer and K. Showalter. *Phys. Rev. Lett.*, 91(17):174103, 2003.

[5] G. Huber, P. Alstrøm, and T. Bohr. *Phys. Rev. Lett.*, 69(16):2380–2383, Oct 1992.

[6] R. Braun and F. Feudel. *Phys. Rev. E*, 53(6):6562–6565, Jun 1996.

[7] F. H. Willeboordse. *Physical Review E*, 47(2):1419–1422, 1993.

[8] Y.-C. Lai and R. Winslow. *Physical Review Letters*, 74(26):5208–5211, 1995.

[9] B. Hof, J. Westerweel, T. M. Schneider, and B. Eckhardt. *Nature*, 443(7107):59–62, 2006.

[10] A. Politi, R. Livi, G.-L. Oppo, and R. Kapral. *EPL (Europhysics Letters)*, 22(8):571, 1993.

[11] D. Ruelle. *Comm. Math. Phys.*, 87(2):287–302, 1982.

[12] D. Ruelle. *Chaotic Evolution and Strange Attractors*. Cambridge University Press, New York, 1989.

[13] M. C. Cross and P. C. Hohenberg. *Rev. Mod. Phys.*, 65(3):851, Jul 1993.

[14] H. S. Greenside. Spatiotemporal chaos in large systems: the scaling of complexity with size. In *Semi-analytic methods for the Navier-Stokes equations (Montreal, QC, 1995)*, volume 20 of *CRM Proc. Lecture Notes*, pages 9–40. Amer. Math. Soc., Providence, RI, 1999.

[15] S. Ruffo. Lyapunov Spectra in Spatially Extended Systems. In *Cellular automata and complex systems (Santiago, 1996)*, pages 153–180. Kluwer Acad. Publ., 1999.

[16] S. Tajima and H. S. Greenside. *Phys. Rev. E*, 66(1):017205, Jul 2002.

[17] M. P. Fishman and D. A. Egolf. *Phys. Rev. Lett.*, 96(5):054103, 2006.

[18] T. Tél and Y. C. Lai. *Physics Reports*, 460(6):245 – 275, 2008.

[19] R. Wackerbauer. *Phys. Rev. E*, 76(5):056207, 2007.

[20] R. Wackerbauer and S. Kobayashi. *Phys. Rev. E*, 75(6):066209, Jun 2007.

[21] J. Crutchfield and K. Kaneko. *Physical Review Letters*, 60(26):2715–2718, 1988.

[22] P. Gray and S. K. Scott. *Chem. Engin. Sci.*, 39(6):1087 – 1097, 1984.

[23] M. Bär and M. Eiswirth. *Phys. Rev. E*, 48(3):R1635–R1637, Sep 1993.

[24] J. H. Merkin, V. Petrov, S. K. Scott, and K. Showalter. *Phys. Rev. Lett.*, 76(3):546–549, Jan 1996.

[25] M. G. Zimmermann, S. O. Firle, M. A. Natiello, M. Hildebrand, M. Eiswirth, M. Bär, A. K. Bangia, and I. G. Kevrekidis. *Physica D: Nonlinear Phenomena*, 110(1-2):92 – 104, 1997.

[26] M. Or-Guil, J. Krishnan, I. G. Kevrekidis, and M. Bär. *Phys. Rev. E*, 64(4):046212, Sep 2001.

[27] M. Meixner, S. Bose, and E. Schöll. *Physica D*, 109(1-2):128 – 138, 1997.

[28] G. Benettin, L. Galgani, and J.-M. Strelcyn. *Phys. Rev. A*, 14(6):2338–2345, Dec 1976.

[29] S. Yonker and R. Wackerbauer. *Physical Review E*, 73(2), 2006.

[30] Oseledets theorem. `http://en.wikipedia.org/wiki/Oseledets_theorem`, Feb 2010.

[31] T. S. Parker and L. O. Chua. *Practical numerical algorithms for chaotic systems*. Springer-Verlag, 1989.

[32] G. H. Golub and C. F. V. Loan. *Matrix Computations (Johns Hopkins Studies in Mathematical Sciences)(3rd Edition)*. The Johns Hopkins University Press, 3rd edition, 10 1996.

[33] E. Ott. *Chaos in Dynamical Systems*. Cambridge University Press, 2 edition, 9 2002.

[34] B. R. Hunt, E. Ott, and J. A. Yorke. *Phys. Rev. E*, 54(5):4819–4823, Nov 1996.

[35] T. Tél. Transient chaos. In B.-L. Hao, editor, *Directions in chaos (3)*. World Scientific, 1990.

[36] A. Pikovsky and A. Politi. *Nonlinearity*, 11(4):1049, 1998.